Modelling Tensile/Compressive Strength Ratio of Artificially Cemented Clean Sands

A. Diambra, PhD, MEng**,** Lecturer**,** Queen's School of Engineering, University of Bristol, Bristol, UK

L. Festugato, PhD, MEng**,** Lecturer, Engineering School, Federal University of Rio Grande do Sul, Porto Alegre, Brazil

E. Ibraim, PhD, MEng**,** Reader, Queen's School of Engineering, University of Bristol, Bristol, UK

A. Peccin, MEng, Engineering School, Federal University of Rio Grande do Sul, Porto Alegre, Brazil

N. C. Consoli, PhD, MEng**,** Professor, Engineering School, Federal University of Rio Grande do Sul, Porto Alegre, Brazil

Revised manuscript submitted for publication to:

Soils and Foundations

on September 2017

Author to receive correspondence: Dr Andrea Diambra
Senior Lecturer in Geomechanics
Queen's School of Engineering
University of Bristol
Bristol (UK)
andrea.diambra@bristol.ac.uk

Number of words: 4500 approx
Number of figures: 9
Number of tables: 3

ABSTRACT:

The present work proposes a new theoretical model for predicting both the splitting tensile (q_t) and compression strengths (q_u) of artificially cemented sands and assesses their ratio for a given material. The proposed developments are based on the concept of superposition of failure strength contributions of the sand and cement phases. The sand matrix obeys the critical state soil mechanics concept, while the strength of the cemented phase can be described using the Drucker-Prager failure criterion. The analytical solutions are challenged against experimental tests on three different cemented clean sands, cured for different time periods. While the analytical relation fits well the experimental data, it also provides a theoretical basis for the explanation of some features related to the experimentally derived strength relationships for cemented clean sands. The value of the power relationship between strengths and the porosity/cement ratio index seems governed by soil matrix properties, while the dependency between the strengths and the curing time can also be captured. For a given cemented sand, the model equally confirms the existence of a unique tensile/compressive strength (q_t/q_u) ratio, independent of the curing time and primarily governed by the compressive to tensile strength ratio (or the friction properties) of the cement. It is also confirmed that the q_t/q_u ratio changes within a narrow range for different frictional properties of the cementing phase.

Keywords: Modelling, sands, Portland cement, tensile strength, compressive strength, porosity/cement ratio.

1 INTRODUCTION

Improving the mechanical characteristics of soils by mixing with small amounts of binding agents, such as cement, is employed worldwide to foster the reuse of locally available soils and decrease construction costs. The main purpose of this ground improvement technique is to reproduce the stable internal structure of naturally cemented or weakly bonded soils, resulting in an increased stiffness and peak frictional strength (e.g. Saxena and Lastrico 1978; Dupas and Pecker 1979; Clough et al. 1981) as well as in the development of some tensile strength (e.g. Leroueil and Vaughan 1990; Clough et al. 1981). These mechanical improvements generally come at the limited expense of a pronounced post-peak brittleness (e.g. Abdulla and Kiousis 1997a; Wang and Leung 2008), caused by the breakage of the artificial cementing bonds during loading.

The addition of cementing agents, especially Portland cement, has been widely adopted in many geotechnical applications to control excessive displacements or settlements of shallow foundations, in slope protection for earth dams, to prevent liquefaction of loose granular soils and in subgrades and base courses for roads and airfield (e.g., Saxena et al. 1988; Porbaha et al. 1998; Gallagher and Mitchell 2002; Thomé et al. 2005; Mitrani and Madabhushi 2010). The technique seems particularly beneficial when applied as a compacted stratum on the top of weak soil layers (Consoli *et al.*, 2009a). Consoli *et al.* (2009a) has shown that the failure mechanism of cemented sand top layers vertically loaded with plates is triggered once the tensile stresses at the bottom of the cemented top layer reach the tensile resistance of the material. Faro *et al.* (2015) has shown that cement treated sand layers built around the top of laterally loaded piles collapse due to the development of excessive compressive stresses. All the above mentioned geotechnical applications have in common a low confining stress level and in these situations the compressive and tensile strength characterisation of the cemented

78 soil from unconfined compression and splitting tensile tests can offer relevant data for the
79 appropriate design of cement-soil mixture (e.g., Gomez and Anderson 2012).

80 Possible dosage methodologies of sand-cement blends must consider the effect of distinctive
81 variables (e.g. quantity of cement and porosity). Based on laboratory experiments, Consoli *et*
82 *al.* (2009b) found out an index named porosity/cement ratio (η/C_{iv}) that plotted against
83 unconfined compressive strength (q_u) defines a power relationship for a given clean sand and
84 Portland cement type under unsaturated conditions (i.e low moisture contents in which pores
85 of the sample are not predominantly water filled during fabrication (Consoli et al. 2009c)) of
86 the following form:

87 $$q_u = X\left[\frac{\eta}{C_{iv}}\right]^Z \quad (1)$$

88 where porosity (η) is expressed as percentage of the volume of voids divided by total volume
89 of the specimen while volumetric cement content (C_{iv}) is expressed as percentage of the volume
90 of cement divided by the total volume of the specimen. X and Z are material parameters that
91 dependent on the sand and binder type. Volume changes during curing are neglected in this
92 approach. Consoli *et al.* (2010) have experimentally extended and confirmed the usefulness of
93 such index in controlling the splitting tensile strength (q_t) of artificially cemented sands. They
94 employed the same sand and Portland cement as used in previous research, and a power
95 relationship with similar shape was obtained:

96 $$q_t = Y\left[\frac{\eta}{C_{iv}}\right]^Z \quad (2)$$

97 where Z appears to retain the same value as for the compression case (1), while Y parameter
98 shows a distinct value from X. In order to check if a q_t/q_u relationship was a function of the
99 porosity, cement content or porosity/cement ratio, Consoli *et al*. (2010) deduced experimental

relationships of types (1) and (2) for Osorio sand – Portland cement blend and then divided the relation(2) by (1), yielding a scalar:

$$\frac{q_t}{q_u} = \frac{4{,}266\left[\frac{\eta}{C_{iv}}\right]^{-1.30}}{28{,}327\left[\frac{\eta}{C_{iv}}\right]^{-1.30}} = 0.15 \qquad (3)$$

This result indicates that there is a straight proportionality between tensile and compressive strengths, and this relation is independent of porosity, cement content and porosity/cement ratio, and that was valid for the whole studied porosity and cement ranges (see Fig. 1 for Osorio sand – Portland cement blend).

The q_t/q_u ratio of artificially cemented granular soils is an important parameter that allows the estimation of q_t knowing q_u or vice versa, considering the whole porosity and volumetric cement content studied. Besides, Consoli (2014) has shown a theoretical framework proving that the friction angle of cemented granular soil is unique for a given soil and cement and its value is a function only of q_t/q_u ratio. Conversely, the cohesion of cemented granular soil can be determined if both q_u and q_t/q_u are known. Floss (2012) extended such studies to other clean sands (a gravelly sand and a sand derived from crushed basalt) treated with Portland cement. The result trends by Floss (2012) were similar to those obtained by Consoli *et al*. (2010): the q_t/q_u relationship of the two clean sands treated with cement yielded distinct scalars ranging from 0.15 to 0.18.

While a few constitutive models have been proposed for predicting the complete mechanical behaviour of cemented sands (e.g. Abdulla and Kiousis, 1997b; Sun and Matsuoka, 1999; Vatsala et al., 2001 and Gao and Zhao, 2011), the empirical relationships in Eqs (1), (2) and (3) provide simple means to predict the unconfined compressive and tensile strengths of cemented soils and their ratio, that can be used for dosage determination of sand-cement blends. To increase confidence for the broader use of such empirical relationships, Diambra et al.

(2017) have developed a theoretical framework based on the superposition of the individual failure strength contributions of both constituents to link the empirical coefficients X and Z governing the unconfined compressive strength (q_u) to both sand and cement properties. The present paper extends such theoretical framework to the prediction of tensile strength (q_t) of cement-sand blends and it theoretically corroborates the experimental observations on the existence of a ratio q_t/q_u, independent of moulding density and cement content, for three different cemented materials cured for different time periods. Insight on the constituents' physical parameters role on controlling the strength of the cemented soil and the q_t/q_u ratio is also explored.

2 THEORETICAL MODEL

2.1 Testing boundary and stress conditions

Typical boundary stress and strain conditions for the unconfined compression and the splitting tensile tests at failure are shown in Fig. 2. The unconfined compression test presents axisymmetric testing conditions (Fig. 2a) and the failure strength (q_u) is equal to the vertically applied stress (σ_z). The stress and strain conditions of a splitting tensile test are slightly more complex. A cylinder is placed horizontally and loaded along its cross-section diameter and plane strain loading conditions (ε_y=0) result on this section (Fig. 2b). Stress conditions are invariably not uniform within the loaded specimen but we could concentrate on a small finite element at the centre of a cross-section disk. The vertical and horizontal principal stresses on this element, σ_z and σ_x, equal $3q_t$ and q_t, respectively, as theoretically demonstrated by Jaeger *et al.* (2007).

The stress state for both tests could be expressed in terms of the maximum shear, t, and mean, s, stress invariants [$t= (\sigma_z- \sigma_x)/2$; $s= (\sigma_z+ \sigma_x)/2$]. By imposing the boundary stress conditions

for both loading cases shown in Fig. 2, the stress ratios at failure for the unconfined compression (k_u) and splitting tensile (k_t) tests at failure can be expressed respectively as:

$$k_u = \frac{t_u}{s_u} = 1 \quad (4)$$

$$k_t = \frac{t_t}{s_t} = 2 \quad (5)$$

where the subscripts *u* and *t* of the stress variables (*t* and *s*) distinguish between unconfined compression and tensile testing conditions, respectively.

2.2 Modelling hypothesis

The artificially cemented sand is assumed an isotropic composite material made of two separate constituents, each one obeying to its own constitutive law: the granular sand matrix and the cementing phase. Three main assumptions are further introduced:

1) The behaviour of the composite cemented sand at the failure point is determined by superposing the strength contributions of the two constituent phases (similarly to the stress superposition approach used by Abdulla and Kiousis 1997b and Vatsala et al. 2001);

2) the sand matrix is expected to be close to peak strength conditions when the cementing bonds break, therefore the failure of the composite cemented sand can be determined by imposing simultaneous failure of both the cemented and the sand matrix phases;

3) Strain compatibility between the composite and its two constituent phases, sand matrix and cement, applies (similarly to the parallel spring approach assumed in Vatsala et al. 2001).

By using a volumetric averaging approach (Diambra *et al.*, 2011; Diambra *et al.*, 2013; Diambra and Ibraim, 2015), the stress state of the composite material (*t*,*s*) can be derived from

the failure stress states of the sand matrix (t_m,s_m) and the cementing phase (t_c,s_c) based on the following relationship:

$$\begin{bmatrix} t \\ s \end{bmatrix} = \mu_m \begin{bmatrix} t_m \\ s_m \end{bmatrix} + \mu_c \begin{bmatrix} t_c \\ s_c \end{bmatrix} \quad (6)$$

where μ_m and μ_c are the volumetric concentrations of sand and cement in the composite material, respectively. It should be noted that the volumetric cement concentration μ_c equals C_{iv}/100.

2.3 Failure relations for constituent phases

2.3.1 Cement phase

It is considered that the strength of the cement phase is simply described by the Drucker-Prager failure criterion, which can be expressed in terms of the maximum shear and mean stresses as follows:

$$t_c = b_c + M_c s_c \quad (7)$$

where the terms b_c and M_c represents the intercept and the slope of the failure line in the *t*-*s* stress plane and, using the developments of Consoli et al. (2014), they can be linked to both the uniaxial compressive (σ_c^c) and tensile (σ_c^t) strengths of the cement phase by the following expressions:

$$b_c = -\frac{\sigma_c^c}{\beta+2} \quad (8)$$

$$M_c = \frac{\beta+4}{\beta+2} \quad (9)$$

where β represents the ratio between the uniaxial compression and extension strengths:

$$\beta = \frac{\sigma_c^c}{\sigma_c^t} \quad (10)$$

2.3.2 Granular soil phase

In soil constitutive modelling, it is customary to link the strength of the granular soils with a state parameter (ψ), which quantifies the difference between the current density state from the corresponding one at the critical state (Been and Jefferies, 1985). It is possible to express the state parameter in terms of the material porosity (η for current porosity and η_{cs} for the corresponding porosity at the critical state) using the following definition:

$$\psi = \frac{\eta_{cs}}{\eta} \tag{11}$$

where ψ>1 represents a state on the loose side of the critical state line (CSL), while ψ<1 represents a state on the dense side of the CSL. Thus, the granular soil stress ratio at failure can then be expressed by the following expression:

$$\frac{t_m}{s_m} = M^* = M\left(\frac{\eta_{cs}}{\eta}\right)^a \tag{12}$$

where M^* represents the peak strength, M is the critical state strength and a is a model parameter which links the peak strength to the state parameter, ψ.

2.4 Strength relationship for artificially cemented sand

By substituting equations (6), (7) and (12) into equations (4) and (5) for the composite stress paths, it is possible to obtain the following expressions for the maximum shear stresses t_u and t_t for unconfined compression and splitting tensile testing conditions, respectively:

$$t_u = \mu_c\left(\frac{b_c + M_c\, s_{c_u} - M^* s_{c_u}}{1 - M^*}\right) \tag{13}$$

$$t_t = 2\mu_c\left(\frac{b_c + M_c s_{c_t} - M^* s_{c_t}}{2 - M^*}\right) \tag{14}$$

However, these relationships (13) and (14) are dependent on the mean stresses developed on the cement phase (s_{c_u} and s_{c_t} for unconfined compression and splitting tensile strengths, respectively), which are actually unknown at this stage. Considering the low strain level

generally induced during the tests prior to failure, elastic conditions can be generally assumed to prevail up to the failure point (Jaeger *et al*., 2007; Consoli et al. 2009a). Thus, by assuming an elastic behaviour for both the composite and the cementing phases, the developments detailed in the Appendix can be used to determine the mean stress contribution of the cementing phase (s_c) at failure for both testing conditions:

$$s_{c_u} = \frac{b_c}{K_u - M_c} \tag{15}$$

$$s_{c_t} = \frac{b_c}{K_t - M_c} \tag{16}$$

where K_u and K_t describe the stress paths (in terms of t_c/s_c ratio) followed by the cement phase which, according to the developments in the Appendix, can be expressed as:

$$K_u = \frac{2\nu_c\nu - 1 + 2\nu_c - \nu}{2\nu_c\nu - 1 + \nu} \tag{17}$$

$$K_t = 2\frac{2\nu_c - 1}{2\nu - 1} \tag{18}$$

where ν is the Poisson's ratio of the composite cemented soil and ν_c is the Poisson's ratio for the cement phase. By substitution of equations (15) and (16) into (13) and (14) respectively and using equations (8) and (9), the following analytical expressions for the unconfined compressive (q_u) and tensile (q_t) strengths can be obtained, respectively:

$$q_u = 2t_u = \frac{2\,\mu_c\,\sigma_c^c}{(\beta+4) - K_u(\beta+2)}\left(\frac{K_u - M\left(\frac{\eta_{cs}}{\eta}\right)^a}{1 - M\left(\frac{\eta_{cs}}{\eta}\right)^a}\right) \tag{19}$$

$$q_t = \frac{t_t}{2} = \frac{\mu_c\,\sigma_c^c}{(\beta+4) - K_u(\beta+2)}\left(\frac{K_t - M\left(\frac{\eta_{cs}}{\eta}\right)^a}{2 - M\left(\frac{\eta_{cs}}{\eta}\right)^a}\right) \tag{20}$$

Relationships (19) and (20) provide direct expressions of the compressive and tensile strengths of the cemented sand as function of the porosity (η, presented as percentage) and the cement content (μ_c) variables, with $\mu_c = C_{iv}/100$. The relations employ seven parameters: three for the soil matrix (M, η_{cs}, a), three for the cement phase (σ_c^c, β, ν_c), and one for the composite

cemented soil (v), as summarised in Table 1. Since the proposed developments refer to unconfined testing conditions only, it appeared reasonable to consider the soil porosity at critical state η_{cs} independent of the mean stress level and thus a material constant.

3 MODEL PREDICTIONS

The validity of the proposed relationships for the unconfined compression and tensile strengths have been assessed by direct comparison with experimental data obtained on three different cemented sands reported in the literature:

1) Uniform Osorio sand + early strength Portland cement cured at 3, 7 and 28 days (Consoli *et al*., 2010);
2) Gravelly sand + early strength Portland cement cured at 7 days (Floss, 2012);
3) Crushed basalt + early strength Portland cement cured at 7 days (Floss, 2012).

The physical properties and moulding parameters for the three materials are reported in Tables 2 and 3, respectively, while their particle size distribution is shown in Figure 3.

3.1.1 Selection of model parameters

As shown in Table 1, the model requires the calibration of seven parameters: three for the soil matrix, three for the cement phase and one for the composite cemented soil. The values of the constants relative to the sand matrices have been selected based on triaxial experimental results and the assumed values are indicated in Table 1. The critical state friction strength ratio M and the critical state porosity η_{cs} for Osorio sand have been derived from published triaxial tests by Dos Santos *et al*. (2010). The same tests were used to establish a relationship between the peak to critical strength ratio (M^*/M) and the state parameter (ψ) in order to determine the model parameter a governing relation (12) as shown in Figure 4.

In absence of available triaxial test data performed on uncemented gravelly sand and crushed basalt materials, the critical state strength ratio M for these materials was derived by using large

255 strain (post peak) strength values for cemented gravelly sand and crushed basalt samples tested
256 under conventional triaxial compression conditions by Floss (2012) which were found to be
257 0.5 and 0.485, respectively. Unfortunately, the value of the critical state porosity η_{cs} under
258 unconfined testing conditions for these materials could not be derived from the same test
259 results. Thus, a value of critical state porosity η_{cs} corresponding to the average between the
260 minimum, η_{min}, and maximum porosity, η_{max}, has been assumed for simplicity. A similar
261 condition stands for η_{cs} value for the Osorio sand which, in this case, was calibrated
262 independently based on the results from Dos Santos *et al*. (2010). The parameter *a* for
263 uncemented gravelly sand and crushed basalt was also assumed to have a similar value to the
264 one for the Osorio sand.

265 The selection of the model's parameters for the cement phases and the overall composites is
266 more difficult and typical values published in the literature has been assumed as a guidance.
267 As discussed in Diambra et al. (2017), the value of the model's parameter β relative to the
268 cement phase has been chosen based on typical ranges for Portland cement. The assumed value
269 of β = -6 agrees also quite well with results of Leonards (1965), who investigated the static and
270 dynamic frictional properties of plain smooth mortar. Chen et al. (2013) have shown values of
271 β ranging between 5 and 7 and decreasing with increasing porosity of the cement mortar.
272 Extensive experimental characterisation of the elastic properties of cemented soils by Felt and
273 Abram (1957) suggests values of the Poisson's ratio for cemented sand and silts between 0.22
274 and 0.31 with a median value of about 0.26, while typical values of Poisson's ratio for mortar
275 matrix are around 0.20, as suggested by Swamy (1971). Therefore, values of 0.26 and 0.20
276 have been assumed for the Poisson's ratio of the composite material (ν) and the cementing
277 phase (ν_c), respectively, leading to the values of the cementing phase stress ratio of K_u=1.89
278 (relation (17)) and K_t=2.25 (relation (18)). The uniaxial compressive strength of the cement
279 phase (σ_c^c) can be finally determined by matching unconfined compression and splitting tensile

strengths using Eqs (19) and (20) and imposing the values selected above for all the other model's parameters. For each cemented soil blend and curing time, the calibration process has been enforced on three randomly selected unconfined compression and splitting tensile tests. Larger values of strength of the cement phase are associated with fine particles, suggesting that presence of fines may improve the creation of cementing bonds. This calibration procedure resembles the curve-fitting imposed by Abdulla and Kiousis (1997b) and Vatsala et al. (2001) for the calibration of the strength of the cementing bonds in their constitutive modelling developments. A summary of the assumed values for model's parameters for each cemented soil blend is provided in Table 1.

3.1.2 Simulations

Comparison between model simulation and experimental data for the unconfined compression strength (q_u) and splitting tensile strength (q_t) is shown in Fig. 5 for cemented Osorio sand cured for different time periods. The data are presented in the strength versus η/C_{iv} ratio plot while a direct comparison between model prediction and experimental data is proposed in the q_{model} *versus* q_{exp} graphs for each curing time analysed. The model predicts reasonably well the magnitude of both unconfined compression strength and splitting tensile tests, with the latter results largely lower. The hyperbolic relationship between strength and η/C_{iv} ratio is also well captured by the model for both testing modes. The expected gain in strength with the curing period is reproduced by assuming increasing values of the cement strength (σ_c^c) with time as shown in Table 1. This simulates the progressive occurrence of hydration chemical reaction and the formation of stronger interparticle cement bonds with time. The accuracy of the prediction seems to increase with increasing curing time and this may be the results of a larger variability of results at low curing time.

Comparison between model simulation results and experimental data for the cemented crushed basalt and gravelly sand cured at 7 days are reported in Fig. 6. The model again predicts quite

well the hyperbolic relationship while the direct comparison between experimental and predicted compressive and tensile strengths (q_{model}-q_{exp}) shows equally a good correlation.

4 DISCUSSION

4.1.1 Parallelism with empirical formula

The proposed relationships (19) and (20) based on theoretical developments have a different form compared with the empirically based relationships (1) and (2) proposed by Consoli *et al*. (2007) and Consoli *et al*. (2011). It is possible to simplify relationships (19) and (20) by introducing the following approximations to their bracketed terms:

$$\frac{K_u - M*}{1 - M^*} \cong M^*(2.07K_i) \quad (21)$$

$$\frac{K_t - M*}{2 - M^*} \cong M^*(0.93K_i) \quad (22)$$

The use of relationships (21) and (22) allows to consider a linear dependency between the cemented soil strengths (q_u or q_t) and the peak strength of the soil M^* ($M^*=M(\eta_{cs}/\eta)^a$) in equations (19) and (20). After further manipulation, we can obtain the following expressions for the unconfined compression and tensile strengths, respectively:

$$q_u = \frac{4.14\ M\ \sigma_c^c {\eta_{cs}}^a\ K_u}{100\ (\beta + 4 - K_u(\beta+2))} \left(\frac{\eta}{C_{iv}^{\frac{1}{a}}} \right)^{-a} \quad (23)$$

$$q_t = \frac{0.93\ M\ \sigma_c^c\ {\eta_{cs}}^a\ K_t}{100\ (\beta + 4 - K_t(\beta+2))} \left(\frac{\eta}{C_{iv}^{\frac{1}{a}}} \right)^{-a} \quad (24)$$

As shown in Fig. 7, the transformations introduced by the relations (21) and (22) have no significant effect on the model predictions when compared with those given by relations (19) and (20). The relations (23) and (24) are now of similar form with the experimentally derived strength relationships in Eqs. (1) and (2) by Consoli *et al.* (2009b) and Consoli *et al.* (2010) with the exception of a power exponent *1/a* to the C_{iv} term. Nevertheless, it should be noted that for the three materials considered here, the exponent *a* was found to be rather close to unity (a~1.30; $1/a$~0.77) and the power adjustment to the term C_{iv} was not required to fit the experimental data in Consoli *et al*. (2009b) exercise. However, some experimental investigations on cemented materials containing better graded soils (Consoli et al. 2007, Consoli et al 2012) have shown that the consideration of a power exponent $1/a<1$ in the

adjusted porosity/cement ratio ($\eta/C_{iv}^{1/a}$) of relation (1) provides a better fit to the experimental data.

The parameter a of the proposed model corresponds to the power $^{-Z}$ in relations (1) and (2) and it confirms that the same value of the exponent $^{-Z}$ controls the strength in unconfined compression and tension testing conditions. The model also suggests that this parameter is entirely governed by the properties of the soil matrix. On the other hand, the parameters X and Y in (1) and (2) differ between them in the two testing modes, as also confirmed by the modelling developments, and they can be analytically expressed by the following relations:

$$X = \frac{4.14\ M\ \sigma_c^c \eta_{cs}{}^a\ K_u}{100\ (\beta+4-K_u(\beta+2))} \quad (25)$$

$$Y = \frac{0.93\ M\ \sigma_c^c\ \eta_{cs}{}^a\ K_t}{100\ (\beta+4-K_t(\beta+2))} \quad (26)$$

The two terms are governed by a combination of parameters related equally to the soil matrix and the cementing phase.

Parametric analysis

The influence of the constituent's properties on the overall compressive and tensile strengths of the cemented soil composite is investigated by performing a parametric analysis. As shown by Diambra et al. (2017), the assumed stress paths for the cement, K_u and K_t, which depend on both the assumed Poisson's ratios for the cement phase and the composite material, have a minimal influence on the model predictions and it has not been presented in this work. On the other hand, the model parameter η_{cs} is introduced to normalise the actual porosity η and to estimate the current soil matrix strength following Eq. (12). This parameter is an inherent soil property and it can not be controlled.. Thus, the sensitivity analysis is conducted here only for the four most influential model parameters, which are those governing the strength properties of the two constituents: σ_c^c and β for the cement phase, M and a for the soil phase. The effects of varying the value for these parameters within a reasonable range – compressive strength σ_c^c between 10 to 60 MPa, cement strength ratio β between -4 and -8, soil matrix strength between 1.1 and 1.5 and the parameter a controlling the strength to density relationship between 1 and 2 - are reported in Figure 8. Both compressive and tensile strengths are affected in the same way by the variation of the parameters. The strength of the cement phase, σ_c^c, appears to be by far the most influential parameter (Fig. 8 a and b), corroborating the widespread knowledge that the selection of the cement type is indeed fundamental for ensuring adequate strength

performances. Selecting a soil matrix with better frictional properties may also marginally improve the strength of the cemented soil for the same amount of cement and compaction degree (Fig. 8 e and f) but any strength improvement is not comparable for what can be achieved by selecting a stronger binding agent. Some caution should be placed when assessing the effect of the parameter *a* (Fig. 8 g and h), since it has a direct connection with the adjusted porosity cement ratio $\eta/C_{iv}^{1/a}$ on the x-axis. Overall, choosing a soil matrix with higher values of *a* (such as a well graded sand as discussed in Diambra et al., 2017) may have some beneficial improvement on strength but still rather limited if compared to the effect of the strength of the cementing phase.

4.1.2 Tensile to compressive strength ratio

The combination of (23) and (24) allows obtaining an explicit relationship that links both tensile and compressive strengths of the cemented soil:

$$\frac{q_t}{q_u} = \frac{2.07K_t\left(\beta+4-K_u(\beta+2)\right)}{1.86\,K_u\ \ \left(\beta+4-K_t(\beta+2)\right)} \tag{26}$$

This relation is mainly dependent on the strength contribution of the cement phase through the slope stress paths, K_u and K_t, and the ratio between the uniaxial compression and tensile strengths of the cementing phase, β, which actually governs the friction ratio of the cementing phase, M_c, through Eq. (9). Direct substitution of the parameters used in this study for the three investigated cemented materials leads to a value of $q_t/q_u = 0.145$, independent of the allowed curing time. This value compares well with the $q_t/q_u = 0.15$ suggested by the experimental data of Consoli *et al*. (2010) for Osorio sand, and with the $q_t/q_u = 0.16$ and $q_t/q_u = 0.18$ for cemented gravelly sand and crushed basalt experimentally found by Floss (2012).

As shown in the Appendix and by the Eqs. (17) and (18), the slopes K_u and K_t of the cement stress paths (governing the q_t/q_u ratio) are dependent on the assumed values of the Poisson's ratio for the composite soil v and the cementing phase v_c. However, variation of these values within the reasonable spectrum (v=[0.2-0.31]; v_c=[0.2-0.3] with $v > v_c$) resulted in rather limited variation of the q_t/q_u ratio between 0.139 and 0.147. The value to be adopted for the cement strength ratio, β, which proves indeed of more difficult, has instead a higher effect on the q_t/q_u ratio. The trend of the overall tensile to compression cement ratio with the parameter β and the corresponding friction angle of the cement phase $\phi_c = asin(Mc)$ is projected in Figure 9. Reasonable variation of the parameter β, to obtain friction angles for the cement phase between

about 20º to 42º, would produce a q_t/q_u ratio between 0.12 and 0.17, which is close to the experimental observed values by Floss (2012) and Consoli et al. (2012).

5 CONCLUSIONS

Theoretical derivations for both unconfined compression and splitting tensile strengths have been developed based on the concept of superposition of failure strength contributions of the soil matrix and cementing phases. Comparisons of model predictions with experimental data for three cemented clean sands and different curing times have shown the validity of the theoretical developments which capture the hyperbolic relationship between the strength and the porosity/cement ratio for both unconfined compression and splitting tensile test conditions. The model also provides some useful insights into the role of some material parameters on the behaviour of cemented sands:

- Corroborating experimental findings, the hyperbolic relationships of unconfined compression (q_u) and splitting tensile (q_t) strengths versus the porosity/cement ratio (η/C_{iv}) are characterised by a similar exponent Z (i.e. Eqs (1) and (2)). The proposed model suggests that such exponent is controlled by the properties of the soil matrix and it is related to the peak strength-density relationship of the soil.
- The model suggests that the different values of the scalars X and Y, governing the hyperbolic relationships of unconfined compression (q_u) and splitting tensile (q_t) strengths versus the porosity/cement ratio (η/C_{iv}) respectively, are related to the different stress paths followed by the overall composite cemented soil and its constituents. The values are affected by the strength of the cementing binds and the sand matrix, with the first factor much more influential than the latter.
- For all three materials, the model yields to a constant splitting tensile to compression strength ratio (q_t/q_u) for the range of porosities and volumetric cement contents considered. The value of this strength ratio is primarily controlled by the frictional strength of the cementing bonds but it varies within a quite narrow range, corroborating past experimental findings. It also seems independent from the curing time.
- Knowledge of the splitting tensile to compression strength ratio (q_t/q_u) enables the estimation of q_t knowing q_u and viceversa. The friction angle of a cemented granular soils is unique for a given soil and cement and its value is a function only of q_t/q_u ratio. Conversely, the cohesion of cemented granular soil can be determined if both q_u and q_t/q_u are known.

- Because of the simplicity in both use and calibration, relationships of the form of Eqs (1) and (2) will likely still be preferred for practical use in routine engineering work. Nevertheless, the present work has provided meaningful connections between the governing coefficients of the empirical relationships and fundamental material properties, increasing confidence for the use of the empirical formulas and providing further guidance towards the design of specific soil and cement mixtures to satisfy required strength criteria

Acknowledgments

The authors gratefully acknowledge the support provided by the UK Royal Academy of Engineering under the Newton Research Collaboration Programme (Grant reference: NRCP1415/2/2).

APPENDIX. Derivation of cement strength contribution

Experimentally observed stress-strain relationship for cemented soil shows a quasi-elastic behaviour up to the peak strength conditions (Consoli *et al.*, 2009a). In fact, the strain levels at failure are generally very small and elastic conditions have been assumed to determine the stress conditions at failure (Jaeger *et al.* 2007). It is supposed here that both the cemented composite soils and its cemented constituent phase behave under elastic conditions. Therefore, the elastic stress-strain relationship for the cemented soils can be written in the following way:

$$\begin{bmatrix}\varepsilon_x\\ \varepsilon_y\\ \varepsilon_z\end{bmatrix} = \frac{1}{E}\begin{bmatrix}1 & -\nu & -\nu\\ -\nu & 1 & -\nu\\ -\nu & -\nu & 1\end{bmatrix}\begin{bmatrix}\sigma_x\\ \sigma_y\\ \sigma_z\end{bmatrix} \quad \text{(A1)}$$

where E and ν are respectively the Young's elastic modulus and Poisson's ratio of the cemented soil and the material is considered isotropic. By applying the boundary conditions shown in Fig. 2 for unconfined compression ($\sigma_z=q_u$, $\sigma_y=0$, $\sigma_x=0$) and splitting tensile ($\sigma_z=3q_t$, $\varepsilon_y=0$, $\sigma_x=-q_t$) tests, it is possible to derive the following strain field for the composite material as function of the material strength (q_u or q_t):

$$\begin{bmatrix}\varepsilon_x\\ \varepsilon_y\\ \varepsilon_z\end{bmatrix} = \frac{q_u}{E}\begin{bmatrix}-\nu\\ -\nu\\ 1\end{bmatrix} \text{ for unconfined compression tests} \quad \text{(A2)}$$

and

449 $$\begin{bmatrix}\varepsilon_x\\ \varepsilon_y\\ \varepsilon_z\end{bmatrix} = \frac{-q_t}{E}\begin{bmatrix}2\nu^2+3\nu+1\\ 0\\ 2\nu^2-\nu-3\end{bmatrix}$$ for splitting tensile tests (A3).

450 Assuming strain compatibility between the composite material and its constituents, it is
451 possible to impose the strain fields given by (A2) and (A3) in the following elastic stress-strain
452 relationship for the cemented soil material:

453 $$\begin{bmatrix}\sigma_{c_x}\\ \sigma_{c_y}\\ \sigma_{c_z}\end{bmatrix} = \frac{E_c}{(1+\nu_c)(1-2\nu_c)}\begin{bmatrix}1-\nu_c & \nu_c & \nu_c\\ \nu_c & 1-\nu_c & \nu_c\\ \nu_c & \nu_c & 1-\nu_c\end{bmatrix}\begin{bmatrix}\varepsilon_x\\ \varepsilon_y\\ \varepsilon_z\end{bmatrix}$$ (A4)

454 where E_c and ν_c are respectively the Young's elastic modulus and Poisson's ratio of the
455 cemented constituent phase. Thus, expressions for σ_{c_x} and σ_{c_z} in both unconfined
456 compression and splitting tensile testing conditions can be derived and substituted in the
457 conventional definition of the maximum shear and mean stress (t_c, s_c) invariants ($t_c=(\sigma_{c_z}$-
458 $\sigma_{c_x})/2$; $s_c=(\sigma_{c_z}+\sigma_{c_x})/2$), to obtain the following slopes of the stress paths (K_u and K_t for
459 unconfined compression and splitting tensile tests respectively) for the cementing constituents
460 phase during loading:

461 $$K_u = \frac{t_c}{s_c} = \frac{\sigma_{c_z}-\sigma_{c_x}}{\sigma_{c_z}+\sigma_{c_x}} = \frac{2\nu_c\nu-1+2\nu_c-\nu}{2\nu_c\nu-1+\nu}$$ (A5)

462 and

463 $$K_t = \frac{t_c}{s_c} = \frac{\sigma_{c_z}-\sigma_{c_x}}{\sigma_{c_z}+\sigma_{c_x}} = 2\frac{2\nu_c-1}{2\nu-1}$$ (A6)

464 These expressions are function of the Poisson's ratios of the cemented material (v) and
465 cementing phase (v_c) only. Intersection of these stress paths with the failure conditions for the
466 cementing phase in Eq. (7), allows the estimation of mean stress contribution of the cementing
467 phase at failure for both testing conditions, s_{c_u} and s_{c_t}:

468 $$s_{c_u} = \frac{b_c}{K_u-M_c}$$ (A7)

469 $$s_{c_t} = \frac{b_c}{K_t-M_c}$$ (A8).

References

Abdulla, A. A., Kiousis, P. D. 1997a. Behavior of cemented sands – I. Testing. International Journal for Numerical and Analytical Methods in Geomechanics, **21**(8): 533-547.

Abdulla, A. A., Kiousis, P. D. 1997b. Behavior of cemented sands – II. Modelling. International Journal for Numerical and Analytical Methods in Geomechanics, **21**(8): 549-568.

Been, K., Jefferies, M.G. 1985. A state parameter for sands. Géotechnique, 35(2): 99-112.

Chen, X., Wu, S., and Zhou J. 2013. Influence of porosity on compressive and tensile strength of cement mortar. ASCE Construction and Building Materials, 40: 869-874.

Clough, G. W.; Sitar, N.; Bachus, R. C., Rad, N. S. 1981. Cemented sands under static loading. Journal of Geotechnical Engineering Division, **107**(6): 799-817.

Consoli, N.C. 2014. A method proposed for the assessment of failure envelopes of cemented sandy soils. Engineering Geology, 169: 61-68.

Consoli, N.C.; Foppa, D.; Festugato, L., Heineck, K.S. 2007. Key parameters for strength control of artificially cemented soils". Journal of Geotechnical and Geoenvironmental Engineering, **133**(2): 197-205.

Consoli, N.C.; Dalla Rosa, F., Fonini, A. 2009a. Plate load tests on cemented soil layers overlying weaker soil. Journal of Geotechnical and Geoenvironmental Engineering, **135**(12): 1846-1856.

Consoli, N.C.; Viana da Fonseca, A.; Cruz, R.C., Heineck, K.S. 2009b. Fundamental parameters for the stiffness and strength control of artificially cemented sand. Journal of Geotechnical and Geoenvironmental Engineering, 135: 1347-1353.

492 Consoli, N. C., da Silva Lopes Jr, L., Foppa, D., Heineck, K. S. 2009c. Key parameters dictating
493 strength of lime/cement-treated soils. Proceedings of the Institution of Civil Engineers-
494 Geotechnical Engineering, 162(2), 111-118.

495 Consoli, N.C.; Cruz, R.C.; Floss, M.F., Festugato, L. 2010. Parameters controlling tensile and
496 compressive strength of artificially cemented sand. Journal of Geotechnical and
497 Geoenvironmental Engineering, 136: 759-763.

498 Consoli, N.C., Viana da Fonseca, A., Cruz, R.C., Silva, S.R. 2011. Voids/cement ratio
499 controlling tensile strength of cement treated soils. Journal of Geotechnical and
500 Geoenvironmental Engineering, 137: 1125-1131.

501 Consoli, N. C., Samaniego, R. A. Q., Marques, S. F. V., Venson, G. I., Pasche, E., Velásquez,
502 L. E. G. 2016. Single model establishing strength of dispersive clay treated with distinct
503 binders. Canadian Geotechnical Journal (Published Online).

504 Consoli, N. C., Consoli, B. S., Festugato, L. 2014. Mohr-Coulomb failure envelopes of lime-
505 treated soils. Géotechnique, 64(2), 165.

506 Consoli, N. C., Marques, S. F. V., Floss, M. F., & Festugato, L. (2017). Broad-Spectrum
507 Empirical Correlation Determining Tensile and Compressive Strength of Cement-
508 Bonded Clean Granular Soils. Journal of Materials in Civil Engineering, 29(6).

509 Diambra, A., Ibraim, E. Russell, A.R., Muir Wood, D. 2011. Modelling the undrained response
510 of fibre reinforced sands. Soils and Foundations **51**(4): 625-636.

511 Diambra, A., Ibraim, E. Russell, A.R., Muir Wood, D. 2013. Fibre reinforced sands: from
512 experiments to modelling and beyond. International Journal for Numerical and
513 Analytical Methods in Geomechanics, **37**(15): 2427-2455.

514 Diambra, A., Ibraim, E. 2015. Fibre-reinforced sand: interaction at the fibre and grain
515 scale. Géotechnique, **65**(4): 296-308.

516 Diambra, A., Ibraim, E., Peccin, A., Consoli, N.C. and Festugato, L., 2017. Theoretical
517 Derivation of Artificially Cemented Granular Soil Strength. Journal of Geotechnical and
518 Geoenvironmental Engineering, p.04017003.

519 Dos Santos, A.P.S., Consoli, N.C., Baudet, B.A. 2010. The mechanics of fibre-reinforced
520 sand. Géotechnique, **60**(10): 791-799.

521 Dupas, J. M., Pecker, A. 1979. "Static and dynamic properties of sand-cement." J. Geotech.
522 Eng. Div., 105(3), 419–436.

523 Faro, V.P., Consoli, N.C., Schnaid, F., Thomé, A., Lopes Jr, L.S. 2015. Field tests on laterally
524 loaded rigid piles in cemented treated soils. Journal of Geotechnical and
525 Geoenvironmental Engineering, **141**(6), 06015003 doi.: 10.1061/(ASCE)GT.1943-
526 5606.0001296.

527 Felt, E. J., Abrams, M. S. 1957. Strength and elastic properties of compacted soil-cement
528 mixtures. American Society for Testing and Materials Special Technical Publication
529 Portland Cement Association Research and Development Laboratory Bulletin.

530 Floss, M.F. 2012. Strength and stiffness parameters controlling artificially cemented granular
531 soils. Ph.D. Thesis, Federal University of Rio Grande do Sul, Porto Alegre, Brazil (in
532 Portuguese).

533 Gallagher, P. M., Mitchell, J. K. 2002. Influence of colloidal silica grout on liquefaction
534 potential and cyclic undrained behavior of loose sand. Soil Dyn. Earthquake Eng., 22(9),
535 1017–1026

536 Gao, Z., Zhao, J. 2012. Constitutive modelling of artificially cemented sand by considering
537 fabric anisotropy. Computers and Geotechnics, **41**: 57-69.

538 Gomez, N. S., Anderson, D. N. 2012. Soil cement stabilization— Mix design, control and
539 results during construction. ISSMGE - TC 211 Int. Symp. on Ground Improvement IS-
540 GI, ISSMGE TC211 and BBRI, Brussels, Belgium.

541 Jaeger, J.C., Cook, N.G.W., Zimmerman, R.W. 2007. Fundamentals of Rock Mechanics. 4th
542 Edition, Oxford - UK, Blackwell Publishing.

543 Lade, P. V., Overton, D. D. 1990. Cementation effects in frictional materials. Journal of
544 Geotechical Engineering, **115**(10): 1373-1387.

545 Leonards, G.A. 1965. Experimental study of static and dynamic friction between soil and
546 typical construction materials. Technical report AFWL-TR-65-161. Air Force Weapons
547 Laboratory.

548 Leroueil, S., Vaughan, P. R. 1990. The general and congruent effects of structure in natural
549 soils and weak rocks. Géotechnique, **40**(3): 467-488.

550 Mitrani, H., Madabhushi, S. G. 2010. "Cementation liquefaction remediation for existing
551 buildings." Proc. Inst. Civ. Eng. Ground Improv., **163**(2), 81–94.

552 Porbaha, A., Tanaka, H., Kobayashi, M. 1998. "State of the art in deep mixing technology. Part
553 II: Applications." Proc. Inst. Civ. Eng. Ground Improv., **2**(3), 125–139.

554 Saxena, S. K., Lastrico, R. M. 1978. Static properties of lightly cemented sand. Journal of
555 Geotechnical Engineering Division, **104**(GT12): 1449-1464.

556 Saxena, S. K., Reddy, K. R., Avramidis, A. S. 1988. “Liquefaction resistance of artificially
557 cemented sand.” Journal Geotechnical Engineering, 10.1061 /(ASCE)0733-
558 9410(1988)114:12(1395), 1395–1413

559 Sun, D. A., Matsuoka, H. 1999. An elastoplastic model for frictional and cohesive materials
560 and its application to cemented sands. Mechanics of Cohesive-Frictional Materials, **4**(6):
561 525-543.

562 Swamy, R. N. 1971. Dynamic Poisson's ratio of Portland cement paste, mortar and
563 concrete. Cement and Concrete Research, **1**(5): 559-583.

564 Thomé, A., Donato, M., Consoli, N. C., Graham, J. 2005. Circular footings on a cemented layer
565 above weak foundation soil.” Canadian Geotechnical Journal, **42**(6), 1569–1584.

566 Vatsala, A., Nova, R., Murthy, B.S. 2001. Elastoplastic model for cemented soils. Journal of
567 Geotechnical and Geoenvironmental Engineering, **127**(8): 679-687.

568 Wang, Y. H., Leung, S. C. 2008. Characterization of cemented sand by experimental and
569 numerical investigations. Journal Geotechnical Geoenvironmental Engineering,
570 10.1061/(ASCE)1090-0241(2008)134:7(992), 992–1004.

571 **TABLES**

572

573 Table 1. Parameters of the proposed model

Symbol	Variable	Values		
		Osorio sand	**Gravelly sand**	**Crushed basalt**
M	Critical state soil strength ratio	0.54 (ϕ ≈33°)	0.5 (ϕ ≈30°)	0.485 (ϕ ≈29°)
η_{cs}	Critical state soil porosity	42.8	29.1	45.5
a	Parameter governing dependence of soil strength on its density	1.30	1.30	1.30
σ_c^c	Uniaxial compressive strength of the cement	27 MPa (3 days) 35 MPa (7 days) 42 MPa (28 days)	28 MPa	30 MPa
β	Uniaxial compression and extension cement strength ratio	-6	-6	-6
v_c	Cement Poisson's ratio	0.2	0.2	0.2
v	Composite Poisson's ratio	0.26	0.26	0.26

574

575 Table 2. Physical properties of the sand materials (after Consoli et al. (2017))

Soil Type	**Uniform Osorio sand**	**Gravelly sand**	**Crushed basalt**
Specific gravity	2.63	2.51	2.63
Mean particle diameter, D_{50}: mm	0.16	2.0	0.28
Uniformity coefficient, C_u	1.9	13.7	3.2
Curvature coefficient, C_c	1.2	0.2	0.9
Minimum porosity, η_{min}	37.5	23.7	38.3
Maximum porosity, η_{max}	47.4	33.8	51.2
Preponderant minerals	Quartz	Quartz	Plagioclase & pyroxene
Particles degree of roundness	Rounded	Sub rounded	Sub rounded
Particles surface texture	Smooth	Smooth	Rough
Soil classification (ASTM 2006)	SP	SP	SP

576

577 Table 3. Granular soils molding parameters.

Soil	**Uniform Osorio sand**	**Crushed basalt**	**Gravelly sand**
Void ratio (*e*)	0.64, 0.70, 0.78	0.71, 0.84, 0.96	0.65, 0.73, 0.84
Cement content (%)	1, 2, 3, 5, 7, 9, 12	1, 2, 3, 5, 7, 9	1, 2, 3, 5, 7
Cement type	PC III	PC III	PC III
Moisture content (%)	10	10	10
η/C_{iv}	from 7 to 101	from 10.2 to 70	from 12.1 to 88.4

578

LIST OF FIGURES

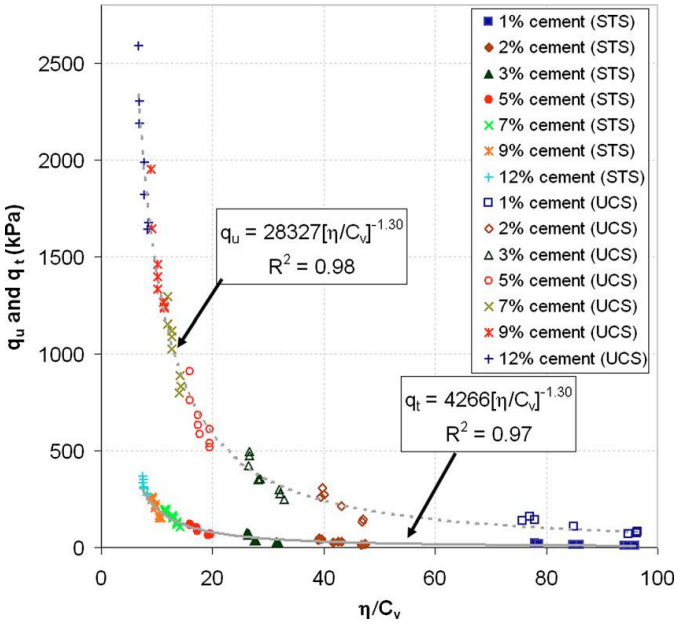

599

600 Figure 1. Variation of q_t and q_u with porosity/cement ratio for Osorio sand – Portland cement (adapted from
601 Consoli *et al.* 2010).

602

603

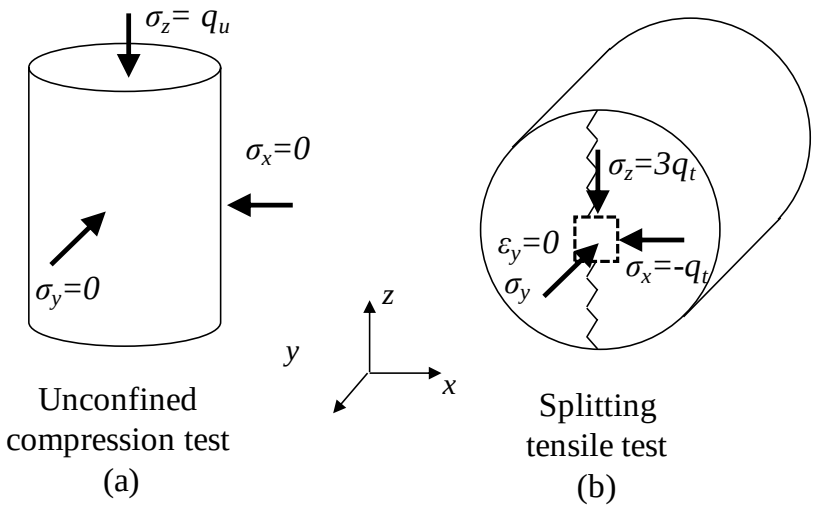

Figure 2. Assumed boundary conditions for (a) unconfined compression test and (b) tensile splitting test.

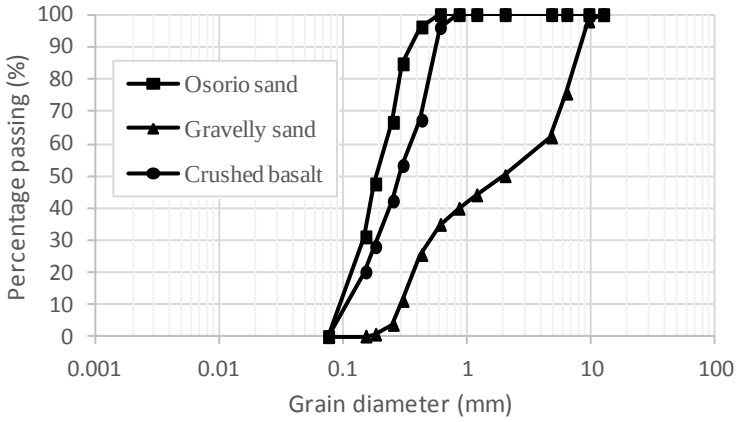

607

608 Figure 3. Particle size distribution for the three studied materials.

609

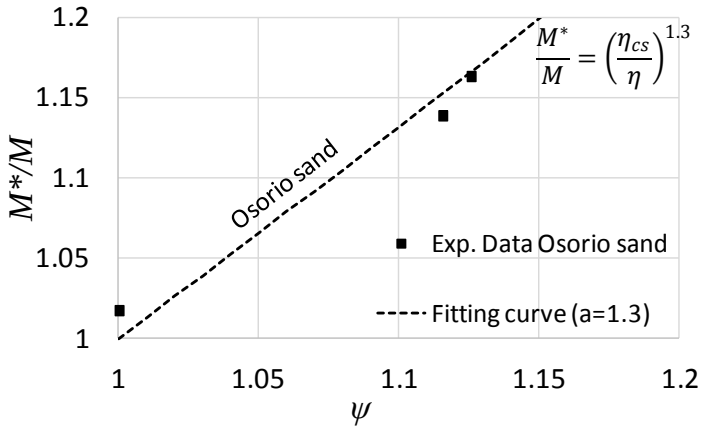

610

611 Figure 4. Calibration of parameter *a* for uncemented Osorio sand using triaxial tests by Dos Santos *et al*. (2010).

612

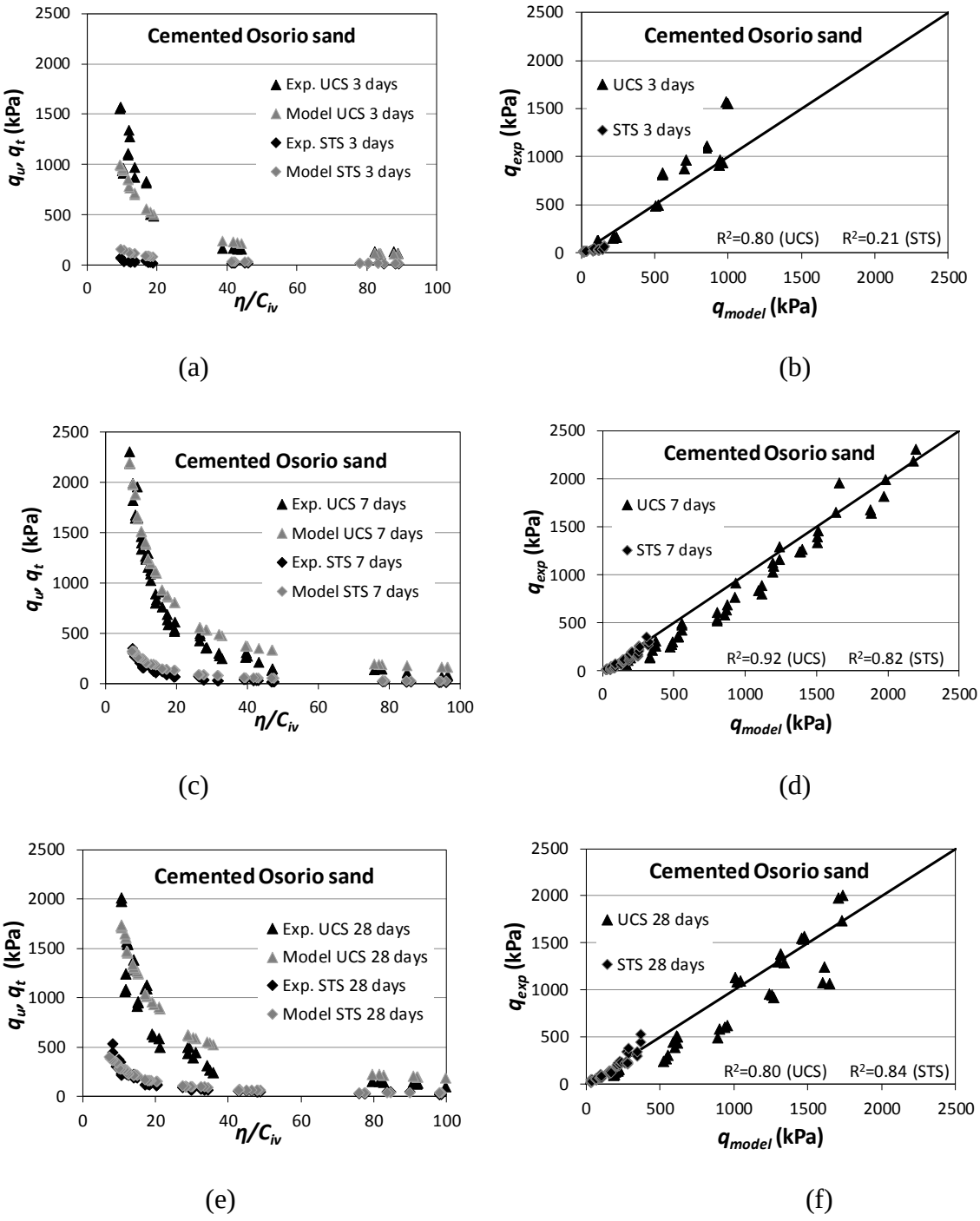

Figure 5. Comparison between model prediction and experimental results for cemented Osorio sand for 7 days: (a–b) 3 days, (c–b) 7 days and (e–f) 28 days.

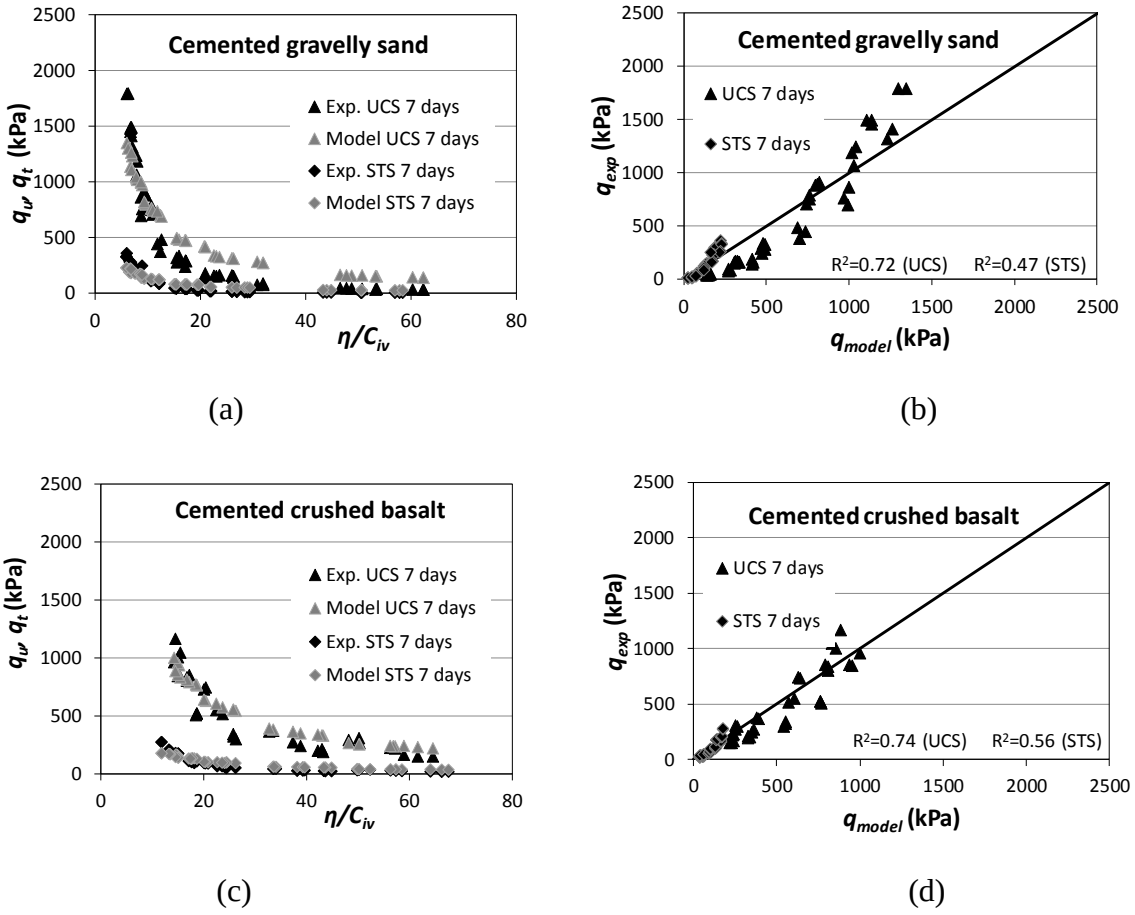

617 Figure 6. Comparison between model prediction and experimental results for (a-b) gravelly sand and (c-d)
618 crushed basalt.

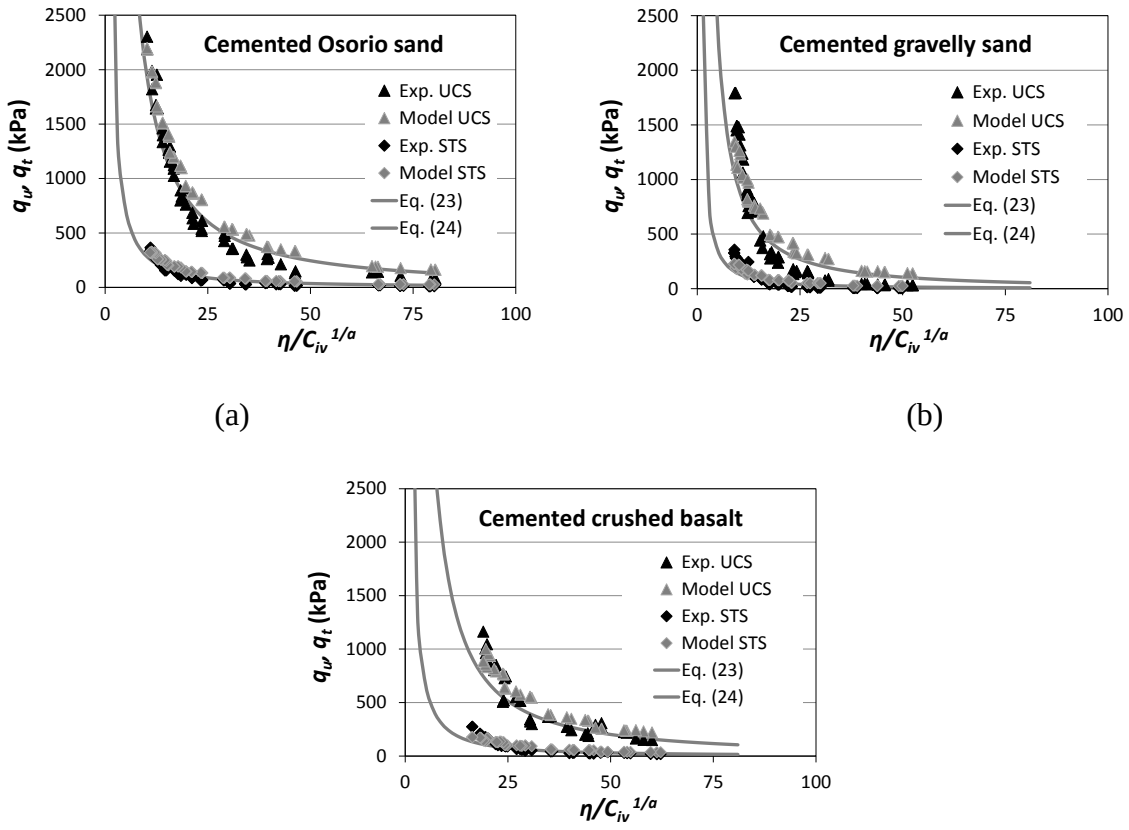

Figure 7. Comparison between experimental data, theoretical prediction and approximated formulas (23) and (24).

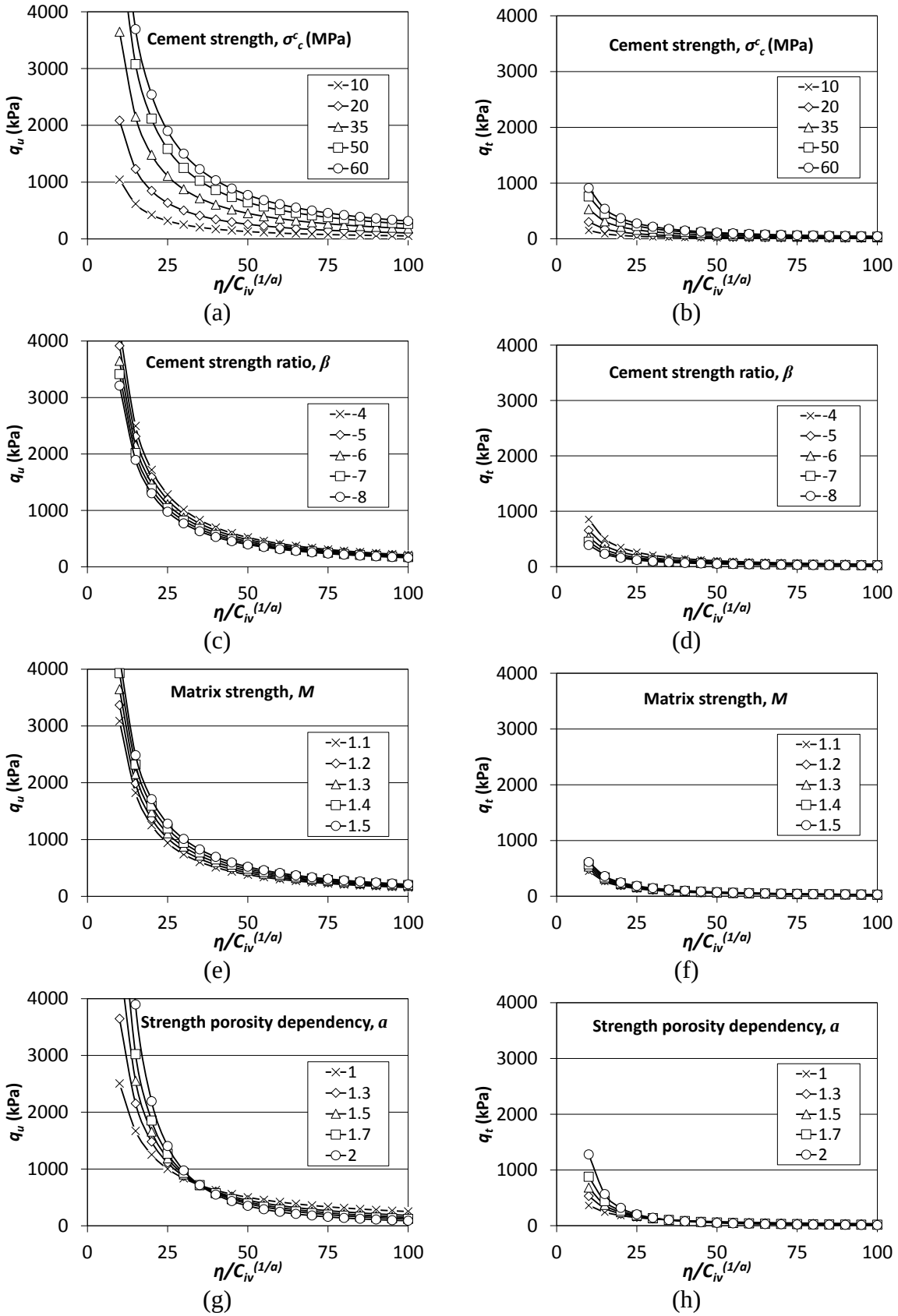

Figure 8. Effect of varying values of morel parameters on both unconfined compressive and splitting tensile strengths prediction: baseline values of the parameters: σ_c^c =35 MPa, β = –6, M = 1.3, and a = 1.3, η_{cs}=35, ν=0.26 and ν_c=0.2.

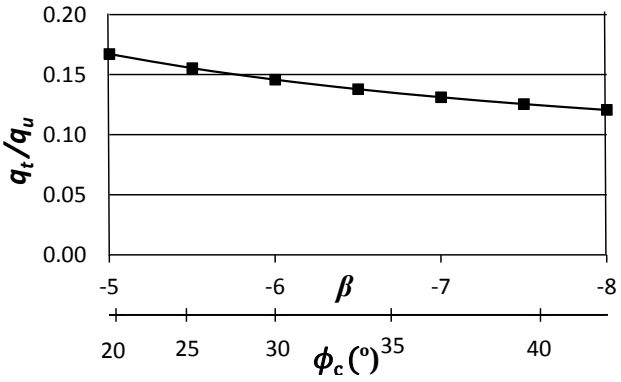

Figure 9. Theoretical variation of q_t/q_u with assumed friction ratio of the cementing phase (β) and corresponding friction angle of the cementing phase (ϕ_c), imposing ν=0.26 and ν_c=0.2.

Notation list

a	Parameter linking peak strength to state parameter
b_c	Cohesion of the cement phase
C_{iv}	Volumetric cement content (expressed in percentage)
M	Critical state strength ratio for the sand in the t -s stress plane
M_c	Slope of the failure line for the cement phase in the t_c -s_c plane
M^*	Peak strength ratio for the sand in the t -s stress plane
k_u	Composite stress ratio at failure for unconfined compression test
k_t	Composite stress ratio at failure splitting tensile test
K_u	Cement stress ratio at failure for unconfined compression test
K_t	Cement stress ratio at failure splitting tensile test
s	Mean stress of the cemented sand
s_c	Mean stress of the cement phase
s_m	Mean stress of the sand matrix
t	Maximum shear stress of the cement sand
t_c	Maximum shear stress of the cement phase
t_m	Maximum shear stress of the sand matrix
q_t	Unconfined compressive strength for the cemented sand
q_u	Unconfined compressive strength for the cemented sand
X	Multiplying parameter in Empirical relationship (1)
Y	Multiplying parameter in Empirical relationship (2)
Z	Exponent of empirical relationships (1) and (2)
β	Uniaxial compression and extension cement strength ratio
ε	Strain for cemented sand
ε_c	Strain for cemented sand

669	ϕ	Friction angle for the sand matrix
670	ϕ_c	Friction angle for the cement phase
671	v	Poisson's ratio for cemented sand
672	v_c	Poisson's ratio for cement phase
673	μ_c	Volumetric cement concentration
674	μ_m	Volumetric sand matrix concentration
675	σ_c^c	Uniaxial compression strength of the cementing phase
676	σ_c^t	Tensile strength of the cementing phase
677	ψ	State parameter
678	η	Porosity
679	η_{cs}	Porosity at critical state